International Journal of Heat and Mass Transfer 52 (2009) 1495–1503

Contents lists available at ScienceDirect

International Journal of Heat and Mass Transfer

journal homepage: www.elsevier.com/locate/ijhmt

Experimental and numerical investigation of the thermal effects during hydrogen charging in packed bed storage tank

G. Momen [a,c], G. Hermosilla [a,b], A. Michau [a], M. Pons [c], M. Firdaous [c], Ph. Marty [b], K. Hassouni [a,*]

[a] Laboratoire d'Ingénierie des Matériaux et des Hautes pressions, 99 Avenue Jean Baptise Clément, 93430 Villetaneuse, France
[b] Laboratoire d'Ecoulements géophysiques et industriels, Domaine Universitaire, BP 53, 38041 Grenoble Cedex 9, France
[c] Laboratoire d'Informatique et de Mécanique pour les Sciences de l'Ingénieur, B.P. 133, 91403 Orsay, Cedex, France

ARTICLE INFO

Article history:
Received 7 December 2007
Received in revised form 5 June 2008
Available online 17 October 2008

Keywords:
Experimental
Packed bed
Thermal effect
Hydrogen storage
Adsorption
Numerical

ABSTRACT

This paper reports on an experimental investigation and numerical simulations of the heating dynamics during hydrogen charging in activated carbon packed bed storage tank. Results showed that the experimentally observed heating dynamics is well predicted using a two-dimensional transport model that makes use of classical averaging rules usually adopted to describe flows in porous media and a linear driving force model to describe the adsorption kinetics. The contribution of the different phenomena to the overall temperature increase of the tank during the charging process was analysed both experimentally and using the developed numerical model. Results showed that the adsorption process is responsible for about 24% of the temperature increase even for moderately adsorbing activated carbon.

1. Introduction

Storage is one of the main issues to the use of hydrogen in mobile applications. The performances of storage technologies are evaluated in term of the gravimetric and volumetric hydrogen densities. The gravimetric density represents the mass percentage of stored hydrogen with respect to the total weight of the tank, while the volumetric hydrogen density corresponds to the mass of hydrogen per unit tank volume. The US Department of Energy (DoE) considers that a viable storage technology should ensure at least 6.5% wt gravimetric density and 65 kg/m^3 volumetric density [1].

Physisorption of hydrogen on micro-porous activated carbons (AC) is being investigated as a possible route for the development of hydrogen storage tank.

In this work we are interested in the performance of activated carbon under practical conditions where a storage tank containing an AC packed bed undergoes a dynamic charging of hydrogen. The dynamic charging of solid tanks is indeed accompanied by a thermal heating due to the exothermal character of the adsorption processes and to the dissipation of the mechanical energy of the gas entering the tank. Since the adsorption capacity of a given material generally decreases when increasing the temperature, this thermal heating leads to a decrease in the storage capacity of the tank. The actual tank performance would therefore substantially differ from what would be obtained assuming a constant temperature. An accurate estimation of the capacity limitation due to this thermal effect can be hardly performed from a simple macroscopic energy balance on the whole tank. This is due to the fact that the heating is not usually uniform over the tank volume. The spatial distribution of the temperature in the tank is therefore not uniform and depends on the interplay between energy transport, energy transfer to the tank wall and heat release in the different locations of the tank.

The estimation of the actual storage capacity of a solid tank when it is used under realistic conditions of a dynamic charging requires therefore a detailed investigation of mass, momentum and energy transport and transfer in adsorbent (carbon) porous packed beds.

We present in this paper experimental and numerical investigation of heat and mass transfers during the charging phase of hydrogen in an activated carbon packed bed storage tank. For this purpose we make use of an experimental set-up that enables performing dynamic charging experiments at pressures as high as 20 MPa. This set-up was especially used to determine the time-evolution of the pressure, the stored quantity of gas and the temperature spatial distribution in the tank during the charging process. The heating dynamics obtained for hydrogen charging experiments were compared to those obtained when helium is used as a feed gas. The purpose here was to qualitatively estimate the contribution of adsorption process to the overall temperature increase observed during the charging process.

* Corresponding author. Tel.: +33 149403411; fax: +33 149403414.
E-mail address: hassouni@limhp.univ-paris13.fr (K. Hassouni).

0017-9310/$ - see front matter © 2008 Elsevier Ltd. All rights reserved.
doi:10.1016/j.ijheatmasstransfer.2008.06.045

Nomenclature

a_s	specific surface area per volume (m^2/m^3)
$C_{v\text{-ads}}$	specific heat of adsorbed molecules (J/kg/K)
$C_{v\text{-H2}}$	specific heat of hydrogen (J/kg/K)
C_s	specific heat of solid bed particles (J/kg/K)
d_P	effective diameter of particle (m)
D_{eff}	effective dispersion coefficient (m^2/s)
E	total energy density (J/m^3)
E_a	adsorption characteristic energy (kJ/mol)
E_g	energy density of the gas fraction in the porous tank (J/m^3)
k	permeability (m^2)
K	mass transfer coefficient (m/s)
M_{H_2}	molar mass of hydrogen (kg/mol)
P	pressure (Pa)
P_0	thermodynamics pressure P^* = dynamics pressure
P_{ch}	charging pressure (MPa)
P_s	saturation pressure (Pa)
P_{lim}	limit pressure (MPa)
$q_{wt\text{-}max}$	mass of adsorbed hydrogen per unit mass of solid bed (kg_{H2}/kg_{solid})
q	amount of adsorbed hydrogen per unit mass of solid bed (mol_{H2}/kg_{solid})
q_{eq}	amount of adsorbed hydrogen per unit mass of solid bed at thermodynamic equilibrium (mol_{H2}/kg_{solid})
q_0	specific amount of adsorbed molecules per unit mass of adsorbent at saturation (mol/kg)
Q_m	inlet mass flow rate (kg/s)
Q_n	inlet volume flow rate (m^3/s)
L_i	tank length (m)
R	universal gas constant (J/mol/K)
R_i	tank radius (m)
S_ρ	mass source term ($kg/m^3/s$)
S_T	heat source generated by the adsorption process ($J/m^3/s$)
S	inlet section of tank (m^2)
T	temperature (K)
$\vec{U} = \begin{pmatrix} \bar{u}_z \\ \bar{u}_r \end{pmatrix}$	velocity vector (m/s)
V	the volume of the tank (m^3)

Greek symbols

γ	Isentropic coefficient
ε_{intra}	intra-particle porosity
ε_t	total bed porosity
ε_h	hydrodynamic porosity
ε_μ	micro-porosity
λ_{eff}	effective conductivity of the packed bed (W/m/K)
μ	gas viscosity (Pa s)
ρ	gas density (kg/m^3)
ρ_s	density of the solid phase (kg/m^3)
ΔH	adsorption enthalpy (J/mol/K)

The results obtained were quantitatively analysed with a two-dimensional numerical model that solves for the non-stationary continuity, momentum and energy equations, which allows simulating the time-evolution of the pressure and the spatial distributions of the temperature and the adsorbed quantities. The model was first validated by comparison with experiment. Then, parametric simulations were used to estimate the contribution of the different heating phenomena to the overall temperature increase observed in the tank.

The present paper is organised in five sections. The next section describes the experimental set-up and procedure used to investigate the time-evolutions of temperature, pressure and flow rate during the dynamic charging process of hydrogen. In Section 3, we present the transport equations used to describe mass, momentum and energy transport in an axi-symmetrical storage tank filled with an AC packed bed. In Section 4, we present the results obtained on the dynamic charging of hydrogen in packed bed reservoir. We also compare between helium and hydrogen charging, which allows estimating experimentally the contribution of adsorption process in the overall heating observed in the tank. The simulation results are also presented in this section. We first discuss the validation of the model in the case of both hydrogen and helium charging for several values of the operating pressure and inlet flow rate. Then we use the model to get a more detailed estimation of the contribution of the different heating mechanism to the overall temperature increase in the tank. The main conclusions that may be drawn from this work are presented in the last section.

2. Experimental set-up and procedure

2.1. Experimental set-up

The experimental set-up presented in Fig. 1 is composed of four parts: the storage tank, a charging circuit, a discharging circuit, and a data-acquisition system.

In the present work, we are interested in the charging phase system, which is described below.

The storage tank is a cylindrical stainless-steel column, with internal and external diameters of 96 and 125 mm, respectively, and an internal length of 255 mm. It is equipped with six thermocouples used to monitor the time-evolution of the temperature at different positions in the tank. The thermocouple positions are defined with respect to the tank inlet ($z = 0$) and to the tank axis ($r = 0$). Thermocouple T1 is located at the entry of the tank ($z = 0$, $r = 0$), T2 at ($z = L/4$, $r = 0$) and T3 at ($z = L/2$, $r = 0$). T4 is located in the vicinity of the tank bottom wall ($z = L$-5 mm, $r = 0$), T5 at the symmetry axis at ($z = L/2$, $r = R_1/2$) and T6 is located at mid-height in the vicinity of the tank side wall ($z = L/2$, $r = R$-2 mm).

The base of the column is equipped with a digital pressure transducer (model DXD 1042, precision: ±0.02% of the full scale) manufactured by Heise able to measure pressure up to 35 MPa.

The gas is fed at the top of the column. The tank inlet is sealed with an insulating tap. The column is packed with activated IRH3 carbon, which has an average surface area of 2600 m^2/g. The IRH3 particles are small cylindrical grains with an effective diameter of 1 mm. The IRH3 activated carbon is produced from coconut coal by the Canadian "*Institut de Recherche sur l'Hydrogène*" [2]. The characteristics of this activated carbon are presented in Table 1.

The charging circuit is composed of a 99.99% purity hydrogen supply that insures a maximum charging pressure of 20 MPa. This supply is equipped with a pressure monitoring system linked through a pipe to the tank. This system enables to maintain a constant inlet pressure with values ranging between 0.1 and 15 MPa during the charging experiment.

The hydrogen inlet flow is measured with a Bronkhorst mass flow-meter (model F-122M-FAB-88-V, precision: ±1% PE), the full-scale of which is 100 l_n/min. This flow-meter is equipped with a regulation valve (B2), which makes possible to control and regulate the hydrogen flow entering the storage tank during the charging phase with a statistical reproducibility of ±0.01%.

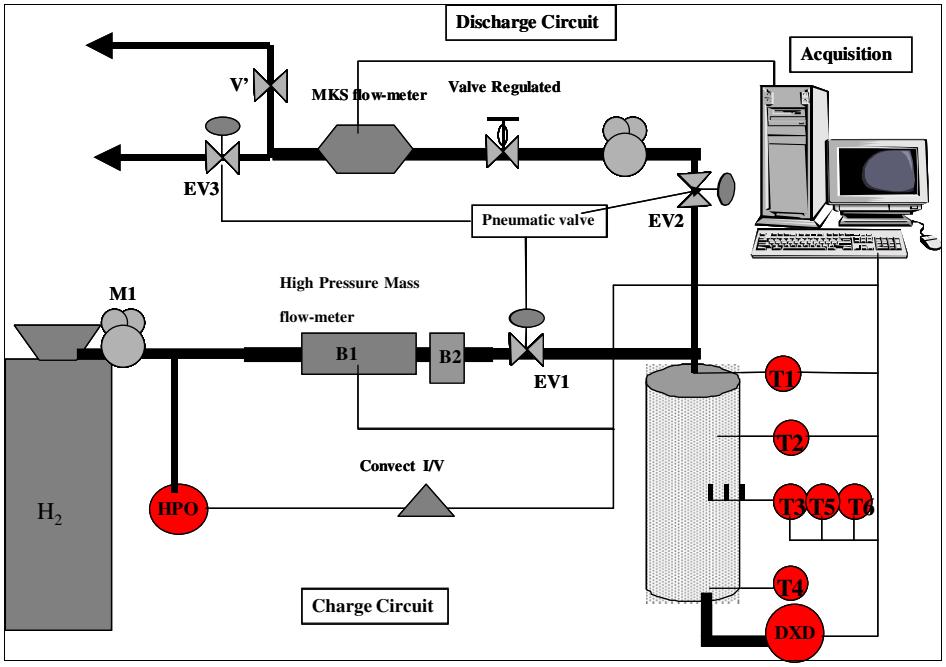

Fig. 1. Experimental set-up.

Table 1
Characteristics of IRH3 activated carbon packed bed

Total porosity	ε_t	0.88	Measured
Hydro-dynamic porosity	ε_H	0.3	Fitted
Solid density	ρ_s (kg/m^3)	1990	Measured
BET Surface area	(m^2/g)	2616	Measured
Bed effective thermal conductivity	λ_{eff} (W/m/K)	0.21	Computed
IRH3 thermal conductivity	λ_{IRH3} (W/m/K)	0.9	Estimated
IRH3 permeability	k (m^2)	3.91×10^{-10}	Measured
Bed effective dispersion coefficient	D_{eff} (m^2/s)	10^{-5}	Computed

2.2. Experimental procedure

Prior to each charging experiment the gas is pumped out from the charging circuit with a primary pump through the manual valve V′ until the pressure reaches a value of 50 mbar. During this phase, the pneumatic valves EV1 and EV2 are closed.

The charging phase takes place in five steps as follows:

- The charging pressure is set at a given value by a high pressure manometer (M1). The charging pressure is the pressure that will be reached at the end of a charging experiment when the steady state is reached in the whole charging circuit including the storage tank.
- The Labview command that allows maintaining the inlet flow rate to a constant value prescribed before starting the experiment is then launched. This Labview command acts on the opening of the regulation valve (B2) to adjust the inlet flow rate to the prescribed value.
- Once the charging pressure and the flow rate value are adjusted, the charging phase starts by opening the pneumatic valve EV1.
- The data's are acquired until the steady state is reached.
- The charging phase is ended by closing the pneumatic valve EV1, when the measured pressure reaches a steady state value that corresponds to the charging pressure. Of course, the flow rate goes to zero at the end of the charging stage when the pressures upstream and downstream the regulation valve are both equal to 10 MPa.

During all this process, inlet mass flow, the pressure at the bottom of the reservoir and the temperature-values at the locations of the six thermocouples are recorded. The data acquisition system includes two multifunction boards (NI PCI-6014) linked to the thermocouples and flow meters through two connecting interfaces (CB-68LP). The data were acquired by means of the Labview (Labview 7.0) software. The acquisition frequencies for the temperatures and pressure are 6.25 and 1 Hz, respectively.

3. Two-dimensional model of gas storage in adsorbent packed bed

The two-dimensional model elaborated in this study enables the prediction of the time-variations of the flow velocity, temperature, adsorption capacity and hydrogen density fields in an axisymmetrical storage tank during the reservoir charging phase.

The time-variation of the hydrogen density, temperature and flow velocity fields are governed by the non-stationary equations of continuity, momentum and energy transport in the porous adsorbent packed bed. These transport equations are obtained by taking the average of the microscopic equations over a representative elementary volume (REV). The following assumptions are made in order to simplify the study and to obtain a closed set of governing equations at the macroscopic scale:

- The porous medium is assumed homogenous and isotropic.
- The solid and gas temperatures are assumed to be equal (thermal equilibrium assumption).
- Hydrogen is assumed to obey the perfect gas law (this assumption is valid below 20 MPa).

Under the above assumptions, the governing equations in the reservoir are expressed in the following sub-sections.

3.1. Hydrogen continuity equation

The mass balance equation of hydrogen can be expressed as:

$$\frac{\partial \rho}{\partial t} = -\mathrm{div}\left[\frac{\rho \cdot \overline{\vec{U}}}{\varepsilon_t - \varepsilon_\mu} - D_{eff}\frac{\vec{\nabla}\rho}{\varepsilon_t - \varepsilon_\mu}\right] + S_\rho \quad (1)$$

where ρ the gas density, $\overline{\vec{U}}$ the hydrogen flow local velocity in the packed bed, ε_μ and ε_t are the micro-porosity and the total porosity, D_{eff} the effective mass dispersion coefficient and S_ρ the adsorption rate of hydrogen.

This equation expresses the balance between the hydrogen accumulation (left-hand side), adsorption (S_ρ) and transport (divergence term) in the tank. In this balance equation we assumed that gaseous hydrogen occupy all the bed porosity except the micro-porosity where only adsorbed hydrogen can be present.

The adsorption source term depends on the bed porosity and the adsorption rate. It may be expressed as:

$$S_\rho = -\frac{1-\varepsilon_t}{\varepsilon_t-\varepsilon_\mu}\rho_s M_{H_2}\frac{dq}{dt} \tag{2}$$

where ρ_s is the bed solid phase density and M_{H_2} the molar mass of hydrogen and q the adsorption capacity of the packed bed. The time-derivative of q represents the overall mass transfer between the solid and gas phase. Its expression may be derived from the Linear Driving Force model using the expression:

$$\frac{dq}{dt} = K\cdot a_s\cdot(q_{eq}-q) \tag{3}$$

where K is the overall mass transfer coefficient, a_s is the specific surface area per unit volume of the porous bed and q_{eq} is the equilibrium adsorption capacity.

The estimation of the source term S_ρ requires determining the equilibrium adsorption capacity q_{eq} over all the pressure and temperature domains experienced in the reservoir during the charging process. The investigated storage conditions correspond to pressures ranging between 0.1 and 10 MPa and temperatures between 295 and 400 K. These temperature and pressure values are higher than those corresponding to the critical values. In such a case adsorption is sometimes referred to as supercritical adsorption. It may be presented through the following extended Dubinin–Astakhov (D–A) equation [3]:

$$q_{eq} = q_0\exp\left[-\left(\frac{RT}{E_a}\ln\left(\frac{P_{lim}}{P}\right)\right)^2\right] \tag{4}$$

In this model, the adsorption capacity depends on three parameters: P_{lim}, E_a, q_0.P_{lim} is the pressure above which the adsorption capacity of the considered material decreases. The adsorption characteristic energy E_a (kJ/mol) and the adsorption capacity at the limit pressure q_0 (mmol/g) depend on the equilibrium temperature. They are expressed as:

$$E_a = \alpha+\beta T \tag{5}$$

$$q_0 = \chi+\delta T \tag{6}$$

The work discussed in this paper was performed on IRH3 activated carbon. The parameters mentioned above are obtained from a best fit with the experimental isotherm reported in [4]. They are listed in Table 2. Typically, the AC considered in this study shows a gravimetric capacity of 0.48% wt, which corresponds to a volumetric capacity of 8.3 kg/m^3, at 298 K and 10 MPa.

3.2. Momentum balance

The fluid velocity is determined from Darcy's law by assuming that the momentum and pressure fields are in equilibrium, i.e., quasi-static assumption [5,6]. The velocity is then given by:

Table 2
Value of the parameters in the modified Dubinin–Astakhov for the investigated IRH3

	α (kJ/mol)	β (kJ/mol/K)	χ (mmol/g)	δ (mmol/g/K)	P_{lim} (MPa)
IRH3	772.92	18.828	7.3235	−0.0088	77.75

$$\overline{\vec{U}} = -\frac{\mu}{k}\vec{\nabla}\cdot P \tag{7}$$

3.3. Energy balance

The energy equation expresses the balance between the amount of energy accumulation in the tank and the energy variations due to convective flow, pressure work, conductive and thermal dispersion fluxes and heat release due to the adsorption process. Under the fluid continuum approach, this balance equation may be expressed as:

$$\frac{\partial E}{\partial t} = -\mathrm{div}(Eg\cdot\overline{\vec{U}}+P\cdot\overline{\vec{U}}) - \mathrm{div}(-[\lambda_{eff}]\nabla T) \tag{8}$$

where E is the total energy per unit volume of the porous bed that includes three components: the gas phase hydrogen energy, the adsorbed hydrogen energy and the bed solid phase energy. It may be expressed as:

$$E = (\varepsilon_t-\varepsilon_\mu)E_g + q\rho_s[1-\varepsilon_t][C_{v\text{-}ads}(T-T_0)+\Delta H]M_{H_2} + [1-\varepsilon_t]\rho_s C_s(T-T_0) \tag{9}$$

where P the total pressure in the reservoir and λ_{eff} the effective thermal conductivity of the bed.

$C_{v\text{-}ads}$ is the specific heat of the adsorbed hydrogen that was assumed to be equal of the specific heat of liquid hydrogen. T is the bed temperature and T_0 is a reference temperature. ΔH is the adsorption enthalpy.The gas energy density is derived assuming a perfect gas low, which means: $E_g = p/(\gamma-1)$ with $\gamma = 7/5$ for H_2.

The energy equation may be expressed in terms of gas temperature:

$$[(\varepsilon_t-\varepsilon_\mu)\rho C_{v\text{-}H2} + q\rho_s[1-\varepsilon_t]C_{v\text{-}ads}M_{H_2} + [1-\varepsilon_t]\rho_s C_s]\frac{\partial T}{\partial t} = -\mathrm{div}(Eg\cdot\vec{U}+P\cdot\vec{U}) - \mathrm{div}(-[\lambda_{eff}]\nabla T) + S_T \tag{10}$$

$C_{v\text{-}H2}$ is the heat capacity of hydrogen;

The source term S_T is linked to S_ρ through the following expression:

$$S_T = S_\rho\frac{\Delta H}{M_{H_2}} \tag{11}$$

As far as bed porosity is concerned, one may distinguish the hydrodynamic inter-particle porosity from the intra-particle porosity.

The hydrodynamic porosity of IRH3 activated carbon was inferred from the measured permeability coefficient, k, using Forchheimer model [6]:

$$k = \frac{\varepsilon_H^3 d_p^2}{150(1-\varepsilon_H^3)} \tag{12}$$

The IRH3 permeability (k) was determined from classical pressure drop vs. flow velocity correlations. We obtained a value of $3.91e^{-10}$ m^2 for this coefficient, which corresponds to a hydrodynamic porosity of 0.3, a value within the admissible range, i.e., 0.25–0.47, for this parameter [7,8].

The total porosity was estimated from simple gravimetric measurements. For this purpose, the effective volume of the IRH3 packed bed was determined, and the porosity was estimated from the ratio of this volume and the IRH3 solid volume computed using the solid density reported in Table 1. A value around 0.88 was found for the total porosity of IRH3. The particle internal porosity was chosen so as to satisfy $\varepsilon_H + \varepsilon_{intra} = 0.88$. It is worthy to mention that a value of 0.1 was reported for the micro-porosity of IRH3 by *Institut de recherche sur l'hydrogène*, Quebec [2].

The heat and mass transfer coefficients were estimated following the procedures reported in references [6,9–11]. The effective

thermal conductivity includes two components: a stagnant component that describes the heat conduction in the absence of convective flow and a *dynamic conductivity*, due to dispersion phenomena that should be taken into account in the presence of convective flow. The stagnant component is estimated from the widely used Zehner–Schlunder correlation, while the dynamic component is estimated as function of the Reynolds number using the correlation reported in [6,9]. For a 0.88 porosity IRH3 packed bed in hydrogen, a value of 0.21 W/m/K was estimated for the effective thermal conductivity. For the range of Reynolds numbers that characterizes the flow in the investigated tank, the dynamic component contributes for less than 5% in the total conductivity value. The effective dispersion coefficient D_{eff} estimated for the investigated charging conditions using the correlation of reference [6,9] is around 10^{-5} m^2/s. With this value, the mass transfer Peclet number, $\frac{\vec{U}d_p}{D_{\text{eff}}}$, can reach values as high as 100 during the early stage of the charging process when the gas velocity is still high.

The main characteristics of the IRH3 packed bed investigated in this work are given in Table 1.

3.4. Numerical solution of the transport equations and simulation procedure

During the storage process the flow inside the reservoir is characterized by a fairly low Mach number and almost spatially uniform pressure field. In this situation, the transport equations (1), (7) and (8) show very high stiffness and cannot be solved in their initial form with the primary variables, i.e., density, velocity and energy [12]. We therefore follow the method suggested in reference [13–15]. The energy equation was expressed in term of pressure. The pressure field was separated in two components. A large time-varying thermodynamic component that is uniform overall the reservoir and a much smaller quasi-stationary hydrodynamic component that governs the flow field in the reservoir [15]. The equation that governs the time-variation of the thermodynamic pressure is derived by integrating the energy equation over all the tank volume. This equation links the time-evolution of the pressure to the inlet flow rate (Q_n). It is expressed as:

$$A\frac{dP_0}{dt} + BP_0 + C = 0 \tag{13}$$

where

$$A = \left[\frac{(\varepsilon_t - \varepsilon_\mu)}{\gamma - 1}V + \rho_s C_{v,s}(1-\varepsilon_t)\frac{M_{H_2}}{R}\iiint_U \frac{dV}{\rho} + q\rho_s C_{v\text{-ads}}(1-\varepsilon_t)\frac{(M_{H_2})^2}{R}\iiint_U \frac{dV}{\rho}\right]$$

$$B = \left(-(1-\varepsilon_t)\rho_s C_{v,s}\frac{M_{H_2}}{R} - (1-\varepsilon_t)\rho_s C_{v\text{-ads}}q\frac{M_{H_2}}{R}\right)\iiint_U \left(\frac{1}{\rho^2}\frac{\partial\rho}{\partial t}dV\right) - \frac{\gamma}{\gamma-1}Q_n$$

$$C = -\left[\lambda_{\text{eff}}\vec{\nabla}\cdot T\right]_{\text{exit}}^{\text{entry}} + \iiint_U (S_\rho\, dV)$$

where V is the tank volume, γ is the isentropic coefficient and P_0 is the thermodynamic pressure.

Once the thermodynamic pressure determined from Eq. (13), the hydrodynamic quasi-static pressure field in the whole reservoir can be estimated from the differential form of the energy equation that may be written [17]:

$$\frac{dP_0}{dt} = \frac{\beta\mu}{(\varepsilon_t - \varepsilon_\mu)\alpha k}\vec{\nabla}\cdot\left(\rho\vec{\nabla}P^*\right) + \frac{\mu\gamma P_0}{k\alpha(\gamma-1)}\Delta P^* + \frac{1}{\alpha} \times \vec{\nabla}\cdot\left(\lambda_{\text{eff}}\vec{\nabla}T\right) + \frac{S_T}{\alpha} + \frac{1}{\alpha}\vec{\nabla}\cdot\left(D_{\text{eff}}\vec{\nabla}\rho\right) \tag{14}$$

where

$$\alpha = \frac{(\varepsilon_t - \varepsilon_\mu)}{\gamma - 1} + \frac{M_{H_2}}{\rho R}(1-\varepsilon_t)\rho_s C_{v,s} + \frac{(M_{H_2})^2}{\rho R}(1-\varepsilon_t)\rho_s C_{v\text{-ads}}q$$

$$\beta = -\frac{(1-\varepsilon_t)\rho_s C_{v,s} M_{H_2} P_0(t)}{R\rho^2} - \frac{(1-\varepsilon_t)\rho_s C_{v\text{-ads}}(M_{H_2})^2 P_0(t)}{R\rho^2}q$$

where μ is the gas viscosity, k is the gas permeability in porous packed bed, P^* is the hydrodynamics pressure.

After this transformation, the charging process can be described by time-integrating the continuity equation (1) and momentum equation (7) coupled to the dynamic pressure Eq. (14) and to the equation that links the time-evolution of the thermodynamic pressure to the inlet flow rate (13). For this purpose these equations are expressed using a finite volume formulation on a 50×50 mesh grid. The dispersion fluxes are estimated using a central difference approximation while the convective fluxes are calculated using an upwind numerical scheme. This formulation leads to the description of the charging process in term of an ordinary algebraic–differential system of equations that govern the time-variation of hydrogen density, gas velocity, dynamic pressure, adsorption capacity and temperature at each grid cell. This ordinary algebraic–differential is time-integrated using LSODE-like solvers based on fully implicit BDF methods [16].

The solution of the equation set requires specifying the initial and boundary conditions. A zero radial gradient boundary condition is adopted at the reactor axis. A zero pressure axial gradient and a constant temperature of 295 K are assumed at the bottom of the reactor. Similarly, zero pressure radial gradient and a constant temperature of 295 K are assumed at the tank wall. In principle, more accurate boundary conditions at the reactor wall may be expressed in terms of energy flux. In this case we specify the balance between the conductive heat flux in the bed at the tank wall and the heat flux transferred from the bed to the tank wall. However, in the situation investigated here, the tank wall is made of steel with very large mass density, a fairly high specific heat and a fairly high conductivity. A rough and very straightforward estimation shows that the total energy produced during the charging process represents less than 2 K temperature increase of the tank wall. It is therefore a good assumption to use a constant temperature boundary condition at the tank wall.

As far as the inlet boundary conditions are concerned two options can be adopted. We can specify the pressure in the reservoir as obtained from experiment (Fig. 2b). In this case Eq. (13) is used to determine the flow rate from the measured time-variation of the thermodynamic pressure. The other option is to specify the flow rate as determined from experimental measurement. In this case, the thermodynamic pressure is determined from Eq. (13). The inlet temperature is set to 295 K.

4. Results and discussion

4.1. Typical pressure and flow rate time-variations during tank charging experiments

Although the charging experiments are performed with an inlet flow rate that is permanently adjusted at a given specified value, the regulation valve cannot ensure a rigorously constant flow rate overall the pressure-variation domain experienced during the charging experiment. As a result, the actual inlet flow rate may significantly deviate from the prescribed value during the charging process. The simulation of the charging process requires the knowledge of the inlet flow rate during the whole charging process. Typical time-variations of the actual inlet flow rate for charg-

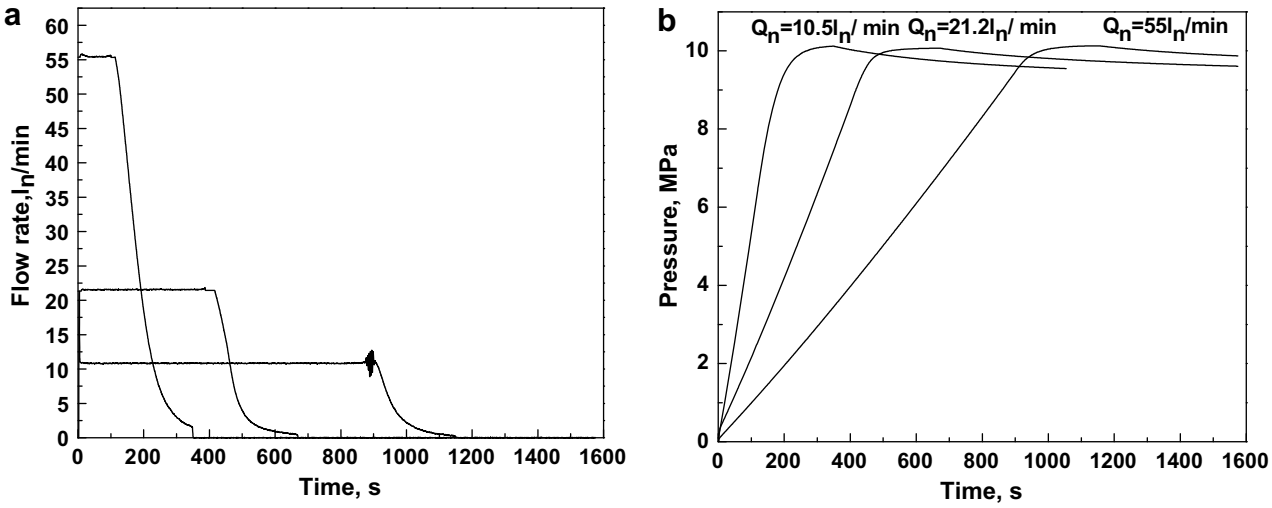

Fig. 2. Time evolution of the flow rate (a) and the pressure (b) obtained during the hydrogen charging phase experiment in an IRH3 AC bed.

ing experiments at a pressure of 10 MPa and several values of the prescribed values of the inlet flow rate are given in Fig. 2a. Fig. 2b shows the corresponding time-variations of the pressure in the storage tank. The charging experiment is characterized by two main phases. The first one corresponds to a constant flow rate value prescribed with the help of the regulation system composed of the mass flow-meter and the regulation valve. Then, we have a fairly short phase where the flow decreases very rapidly to zero. During this second phase the pressure drop through the regulation valve is so small that the flow rate is smaller than the prescribed value even though the regulation valve is fully open. The flow is therefore fully determined by the pressure drops through the different components of the charging circuit (valves, flow-meter and so,...). It therefore decreases with the pressure drops through the components of the charging circuit until an equilibrium situation is reached and the pressure is constant over all the charging circuit and the storage tank.

4.2. Comparison between measured and calculated temperature fields during hydrogen charging experiments

Fig. 3 shows the calculated and measured time-evolutions of the temperatures at position T1, T2, T3, T4, T5 and T6 for a charging experiment performed at a pressure of 10 MPa and inlet flow rate of 17.6 l_n/min.

There is a very good quantitative agreement between the calculated and measured time-evolutions of the temperature in the bulk of the tank (position T3). The difference between the calculated and measured temperature remains indeed below 1 K, i.e., less than 3% of the temperature increase, during the charging experiment. There is also a good agreement between the measured and calculated time-evolutions of the temperatures at positions T2 and T5. The difference between the calculated and measured temperatures remains indeed smaller than 2 K, i.e., less than 10% of the temperature increase at these positions.

A fairly good agreement is also obtained between simulation and experiment for the time-evolution of the temperature at position T4 near the bottom wall of the tank. The difference between measurement and calculation although significant at the beginning of the charging experiment, tends to decrease and becomes rapidly smaller than 1 K.

The agreement between experiment and simulation is somewhat less satisfactory for position T6 located in the vicinity of the lateral wall of the tank. The difference between the predicted and measured maximum temperatures is around 3 K which represents more than 30% of the temperature increase observed during the charging process. This difference may be due to the uncertainty on the exact locations of T6. As a matter of fact, the temperature distribution in the tank is characterized by strong thermal gradients in the vicinity of the wall. This may be clearly seen in Fig. 4 where we reported the temperature distribution at the end of the charging process when the temperature reaches its maximum at position T3. The temperature decreases by approximately 1 K/mm inside the boundary layers in the vicinity of the wall. A small error on the location of position T4 and T6 can therefore result in a significant change in the predicted temperature for these positions.

The numerical model developed in this work was validated for different values of the inlet flow rate and charging pressure.

Fig. 5 shows the time-evolutions of the temperature at position T3 for two prescribed values for the inlet flow rate, i.e., 55 l_n/min and 17.6 l_n/min. A good agreement is obtained between measurements and simulation for the two flow rate values although the agreement is much better at small flow rate for which the temperature difference remains less than 1 K. The temperature difference for the large flow rate value remains below 4 K, which represents 10% of the maximum temperature increase observed during the charging experiment.

It is interesting to notice that the increase of the inlet flow rate, results in a significantly stronger heating since the temperature increase during the charging process varies from 30 K for a flow rate of 17.5 l_n/min to 45 K for a flow rate of 55 l_n/min.

Fig. 6 shows the time-evolutions of the temperature at position T3 for two values of the charging pressure: 10 and 15 MPa. Good agreement between simulation and measurement is obtained for the two charging conditions since the difference between the calculated and measured temperatures remain below 1-2 K during all the charging process. It is interesting to notice that the increase of the charging pressure has only small effect on the maximum temperature achieved in the tank. 30% pressure increase results in only 5 K, less than 15% relative variation, of temperature increase during the charging process.

4.3. Analysis of the overall heating dynamic of the tank and contribution of the heat release due to adsorption in the observed temperature increase

To estimate the contribution of adsorption to the overall temperature increase observed experimentally, we first performed

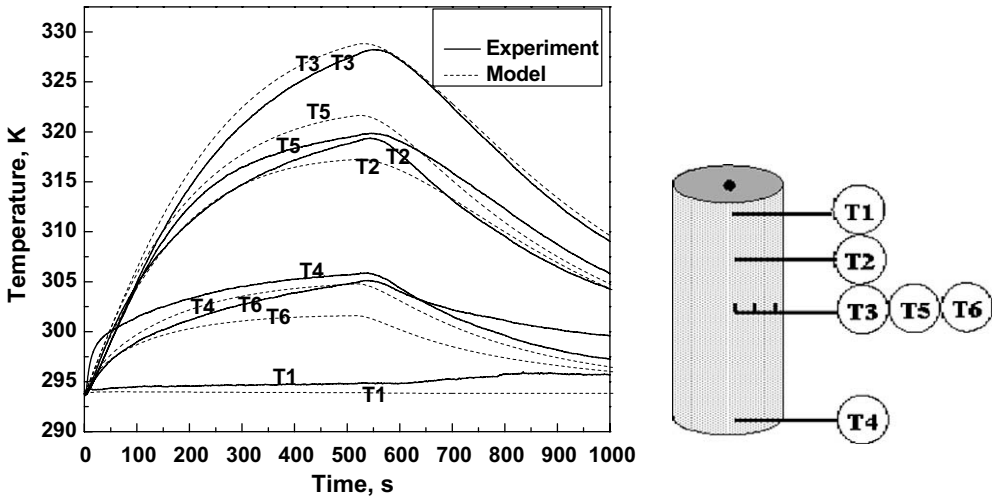

Fig. 3. Calculated and measured evolution of hydrogen temperatures in several positions in the reservoir P_{ch} = 10 MPa, Q_n = 17.6 l_n/min.

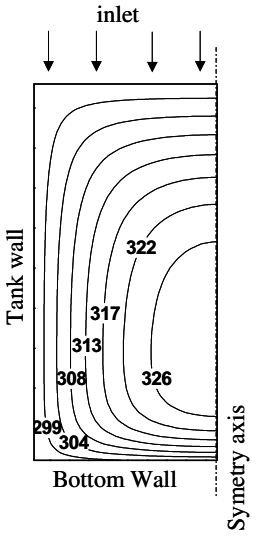

Fig. 4. The temperature field in the tank at the end of the charging process, i.e., t = 550 s, when the temperature at T3 reaches its maximum value. P_{ch} = 10 MPa, Q_n = 17.6 l_n/min.

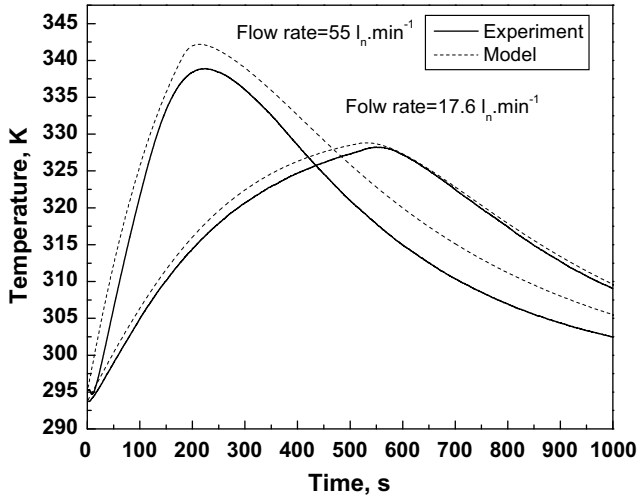

Fig. 5. Comparison of the flow rate effect on the evolution of hydrogen temperature (T3) in the IRH3 packed bed by the model and the experience, P_{ch} = 10 MPa.

some comparison between experiments with hydrogen and helium. Fig. 7 shows the time-evolutions of the temperature in the bulk of the tank (position T3) obtained for helium and hydrogen charging.

The temperature variation is governed by the energy equation (8) where the only terms that are gas nature dependent are the effective conductivity flux divergence and the adsorption source term. Since we are considering the same AC packed bed and since helium and hydrogen conductivities are very close, the effective conductivity flux divergence terms for hydrogen and helium are likely to be very similar. As a result, the only effect that can induce the observed difference between the heating dynamics in helium and hydrogen charging experiments is due to the adsorption source term. If we assume, as generally reported in the literature, that helium adsorption is negligible with respect to hydrogen adsorption, the extra heating observed in the case of hydrogen can be attributed to the heat release due to adsorption.

This effect induces therefore significantly higher temperature in hydrogen, i.e., the maximum temperature achieved during the charging experiment is 10 K higher when using hydrogen. The temperature increase can be considered as quasi-proportional to

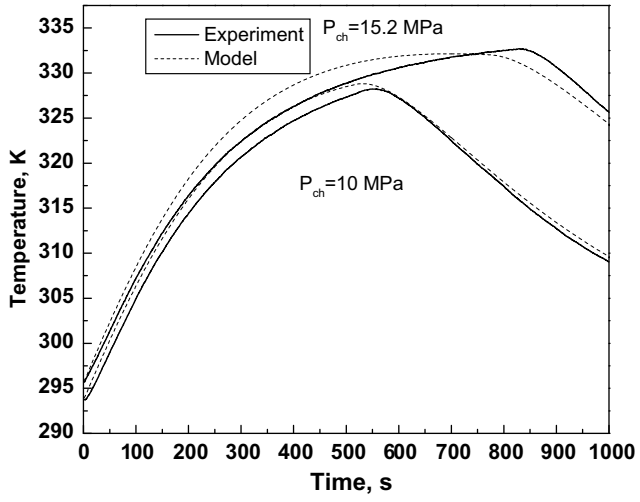

Fig. 6. Comparison of the pressure effect on the evolution of hydrogen temperature (T3) in the IRH3 packed bed by the model and the experience, Q_n = 17.6 l_n/min.

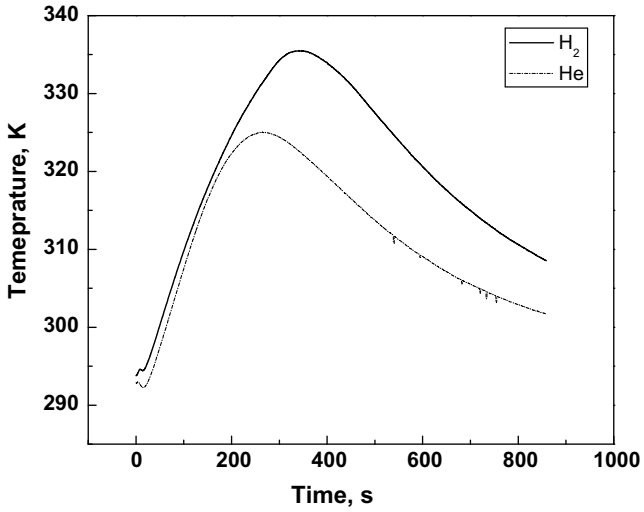

Fig. 7. Comparison of the experimental temperature evolution at the hottest location (T3) obtained with hydrogen and helium charging, Q_n = 30 l_n/min, P_{ch} = 10 MPa.

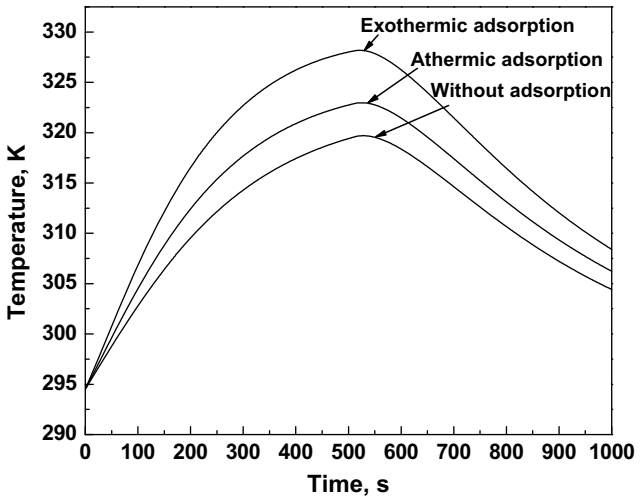

Fig. 8. Analyse of the heat released during the charging process of hydrogen by model, P_{ch} = 10 MPa, Q_n = 17.6 l_n/min.

the thermal energy dissipated in the tank during the heating phase where the energy losses can be neglected. It appears therefore that 76% of the total heating produced during the hydrogen charging is due to the conversion to heat of the energy related to the work of the pressure forces that enables tank charging. At the end, only 24% of the observed 42 K temperature increase is due to adsorption.

Similar analysis was performed using the transport model described in this work, and we performed three simulations to estimate the contribution of the adsorption to the observed overall heating. The first simulation takes into account the adsorption phenomenon with the thermodynamic parameters reported in Table 1 (IRH3 AC). In the second simulation, we used the same adsorption characteristics except for the adsorption enthalpy that we assumed to be zero (no heat generation due to adsorption). In the third simulation we assumed that there is no hydrogen adsorption in the tank.

The difference in the temperature increase between the first and second simulations can be attributed to the energy released by the surface process of adsorption. While the difference between the first and third simulations is not only due to the heat release during the adsorption process but also to a partial conversion to heat of the mechanical work necessary to feed the additional gas quantity stored in the solid phase.

Fig. 8 depicts the time-evolutions of the temperature obtained in the three simulations. It shows that 76% of the total heat released during the charging process is due to the dissipation of the mechanical work necessary to perform the charging process, which is in excellent agreement with the results obtained from the comparison between helium and hydrogen charging experiments. Among the 24% contribution of adsorption, 16% is due to the exothermic characteristic of adsorption process and the remaining 8% comes from the dissipation of pressure works necessary to inject the additional gas quantity stored in the solid phase.

5. Conclusion

The numerical model and experimental study discussed in this paper enabled to analyse the heating dynamics during hydrogen charging in a IRH3 activated carbon packed bed storage tank. Both simulations and experiments showed that the temperature distribution is strongly non-uniform in the tank during the charging process. The measured and simulated time-variations of the temperature in the bulk of the tank are in very good agreement and show a temperature increase of about 40 K for a charging duration of 300 s (5 min) and charging pressure of 10 MPa at ambient temperature in the moderately adsorbing IRH3 packed bed. The temperature keeps increasing during all the charging process and no steady state value is reached for the temperature during the charging phase. This behavior is due to the very slow energy transfer dynamic inside the packed bed. This results in a rate of energy loss at the tank wall that remains smaller than the rate of heat release in the tank, through adsorption and dissipation of the mechanical energy due to the compression forces, during almost all the charging phase. As a result a significant temperature increase during the charging process is obtained. It is noteworthy that such increase was not observed when using a storage tank without any packed bed. In such a situation the energy transfer to the tank wall through convection is quite strong and induces very large heat losses at the tank wall.

Parametric studies performed by modeling and experiments showed that for a given tank geometry and adsorbent packed bed the temperature increase is mainly governed by the charging flow rate. This is determined by the tank volume, the charging pressure and the charging duration. The temperature increase is significantly enhanced when operating at higher flow rate.

Simulation results and comparisons between charging experiments using hydrogen and helium allowed the estimation of the contribution of the different energy sources to the observed overall heating in the tank. With the IRH3 activated carbon packed bed investigated in this work, the adsorption effect account for only 24% of the observed temperature increase. This contribution may become more significant if charging experiments are performed at lower temperature (cryogenic conditions) or with higher performance adsorbent (Maxsorb).

Now that the transport model developed in this work was quantitatively validated by comparison to experiment, it can be used to investigate the heating dynamic under these conditions that show more significant thermal effect.

References

[1] P. Bénard, R. Chahine, Modeling of adsorption storage of hydrogen on activated carbons, Int. J. Hydrogen Energy 26 (2001) 849–855.

[2] http://irh.uqtr.ca.
[3] L. Zhan, K.X. Li, R. Zhang, Improvements of the DA equation for application in hydrogen adsorption at supercritical conditions, J. Supercrit. Fluids 28 (2004) 37–45.
[4] A. Delahaye, Dynamics storage of hydrogen by adsorption on an activated carbon fixed bed using a 2D modelling of heat effects, Ph.D. Thesis, University of Paris 13, 2002.
[5] O. Bey, G. Eigenberger, Fluid flow through catalyst filled tube, Chem. Eng. Sci. 52 (8) (1997) 1365–1376.
[6] M. Weinterberg, E. Tsotsas, A. Krischke, D. Vortmeyer, A simple and coherent of set of coefficients for modeling of heat and mass transport with and without chemical reaction in tubes filled with spheres, Chem. Eng. Sci. 55 (2000) 967–979.
[7] A.S. Afandizadeh, E.A. Foumeny, Design of packed bed reactors: guide to catalyst shape, size, and loading, Appl. Therm. Eng. 21 (2001) 669–682.
[8] E.A. Foumeny, A. Kulkarni, S. Roshani, A. Vatani, Elucidation of pressure drop in packed bed systems, Appl. Therm. Eng. 16 (3) (1996) 195–202.
[9] M. Winterberg, E. Tsotsas, Correlation for effective heat transport coefficients in beds packed with cylindrical particles, Chem. Eng. Sci. 55 (2001) 5397–5943.
[10] C.T. Hsu, P. Cheng, K.W. Wong, Modified Zehner–Schlunder models for stagnant thermal conductivity of porous media, Int. J. Heat Mass Transfer 37 (17) (1994) 2751–2759.
[11] E.L. Smirnov, V.A. Kuzmin, I.A. Zolotraskii, Radial thermal conductivity in cylindrical beds packed by shaped particles, Chem. Eng. Res. Des. 82 (A2) (2004) 293–296.
[12] S.V. Patankar, Numerical Heat Transfer and Fluid Flow, Taylor & Francis, London, 1978. pp. 83–97.
[13] C.D. Munz, S. Roller, R. Klein, K.J. Geratz, The extension of incompressible flow solvers to the weakly compressible regime, Comput. Fluids 32 (2003) 173–196.
[14] I.J. Keshtiban, F. Belblidia, M.F. Webster, Compressible Flow Solvers for Low Mach Number Flows – A Review, Institute of Non-Newtonian Fluid Mechanics, University of Wales, UK, Report No.: CSR 2-2004.
[15] P. Jenny, B. Müller, Convergence acceleration for computing steady-state compressible flow at low mach number, Comput. Fluids 28 (1999) 951–972.
[16] A.C. Hindmarsh, ODEPACK: A systematized collection of ode solvers, in: R.S. Stepleman et al. (Eds.), Scientific Computing, North-Holland, Amsterdam, 1983, pp. 55–64.